

Pattern formation and phase transitions in systems with non-monotonic interaction

H.J. Zhao, V.R. Misko, and F.M. Peeters
*Department of Physics, University of Antwerpen,
Groenenborgerlaan 171, B-2020 Antwerpen, Belgium*
(Dated: April 23, 2022)

We analyzed pattern formation and identified different phases in a system of particles interacting through a non-monotonic short-range repulsive ($r < r_c$) and long-range attractive ($r > r_c$) potential, using molecular-dynamics simulations. Depending on parameters, the interaction potential models the interparticle interaction in various physical systems ranging from atoms, molecules and colloids to neutron stars and vortices in low κ type-II superconductors and in recently discovered “type-1.5” superconductors. We constructed the phase diagram “critical radius r_c – density n ” and proposed a new approach to characterization of the phases. Namely, we elaborated a set of quantitative criteria in order to identify the different phases using the Radial Distribution Function (RDF), the local density function, and the occupation factor.

I. INTRODUCTION

Pattern formation in many systems is governed by competing interaction¹. Examples of such systems are: the pasta phase in neutron stars², ferrofluids^{3–6}, Langmuir monolayers^{7,8}, magnetic garnet thin films, type-I superconductors⁹, colloids and gels^{10–14}, etc. In general, there is a strong correlation between the pattern formation and the inter-particle interaction. Attraction favors aggregation, while repulsion favors low local densities. This competition between repulsive and attractive interaction leads to very rich phases, such as stripes, clusters, bubbles, etc.¹⁵. Those different phases were observed in many diverse systems. In neutron stars, the competition between the short-range nuclear attraction and the long-range Coulomb repulsion leads to complex pasta phases². In ferrofluid systems, rich phases due to the competition between dipolar forces and short-range forces opposing density variations were found experimentally³ and theoretically⁴.

Pattern formation was extensively studied in colloidal systems where the colloid-colloid interaction is characterized by the competition of the hardcore excluded volume interaction, on the one hand, and the polarization of the particles, on the other hand. The interaction potential can be further controlled by adding other components. As a result, rich configurations, such as clusters, repulsive or attractive glassy states, gels, were found numerically^{16–21}, analytically^{22,23} and experimentally^{11,13} in colloidal systems with short range attractive interaction. The properties of isolated clusters formed by the short-range attractive and long-range repulsive interaction were studied²⁴. By controlling the interaction, the growth of the cluster was shown to change from nearly spherical to one-dimensional. The one-dimensional growth of the clusters facilitated the collective packing into columnar or lamellar phases²⁴. The columnar and lamellar phases in three dimension were also studied by molecular dynamics (MD) simulations²⁵.

In superconductors, the vortex-vortex interaction is usually considered to be either repulsive (in type-II superconductors where the Ginzburg-Landau parameter κ ,

i.e., the ratio of the magnetic field penetration depth λ to the coherence length ξ , $\kappa > 1/\sqrt{2}$) or attractive (in type-I superconductors, where $\kappa < 1/\sqrt{2}$ and vortices are unstable) while vortices do not interact with each other at the so-called “dual point” when $\kappa = 1/\sqrt{2}$ ²⁶. However, a deeper analysis of the inter-vortex interaction in type-II superconductors near the dual point revealed an attractive tail^{27,28}. This repulsive-attractive inter-vortex interaction was used for the explanation of unusual patterns in the intermediate state in low- κ superconductors (e.g., Nb): islands of Meissner phase surrounded by vortex phase or vice versa, i.e., vortex clusters surrounded by Meissner phase^{27,28}.

Recent discovery of “type-1.5” superconductors²⁹ induced a new wave of interest (see, e.g., Ref.^{30,31}) to systems with non-monotonic interactions, due to the fact that the observed vortex patterns in those superconductors revealed a clear signature of the repulsive-attractive inter-vortex interaction. In particular, several properties (e.g., vortex lattice with voids, the nearest-neighbor distribution) of the observed vortex patterns were explained using a simple model that involved a non-monotonic inter-vortex interaction based on a more general approach to multi-order-parameter condensates³².

In this paper, we consider a model competing interaction potential which is repulsive for short range and attractive for long range. This form of the interaction potential could be used as a model for different systems with non-monotonic inter-particle interaction, e.g., atoms or molecules (i.e., the Lennard-Jones potential), or vortices in two-band superconductors, depending on specific parameters of the potential. We study pattern formation in two-dimensional systems, for different interaction potential profiles, i.e., we distinguish “soft-core” and “hard-core” interactions and analyze the transitions between different phases. Based on this, we construct a phase diagram for different interaction parameters and particle densities. We propose a new approach to characterize the different phases: instead of qualitative characterization of the phases (e.g., clusters or labyrinths), we introduce a number of quantitative criteria to distinguish these. In particular, different phases are analyzed in terms of

the Radial Distribution Function (RDF) and additional quantities characterizing, e.g., the local density of particles in clusters.

The paper is organized as follows. In Sec. II, we describe the model. The pattern formation for different interaction parameters is discussed in Sec. III. In Sec. IV, we analyze different phases using the RDF and discuss criteria for identification of different patterns. The conclusions are given in Sec. V.

II. MODEL

The inter-particle interaction potential is taken to be of the following form:

$$V_{ij} = V_0 \left(\frac{a}{b} * K_0(b * r_{ij}/\lambda) - K_0(r_{ij}/\lambda) \right). \quad (1)$$

Here, K_0 is a first order Bessel function, $r_{ij} = |\mathbf{r}_i - \mathbf{r}_j|$ is the inter-vortex distance, V_0 and λ are the units of energy and length, respectively. [Note that in case of a type-II superconductor appropriate units of length λ and the energy V_0 , correspondingly, are the magnetic field penetration depth λ and $V_0 = \Phi_0^2/8\pi^2\lambda^2$, where $\Phi_0 = hc/2e$ (see, e.g., Ref.³³)].

In dimensionless form, the interaction potential (1) reads as

$$V'_{ij} = \frac{V_{ij}}{V_0} = \frac{a}{b} * K_0(b * r'_{ij}) - K_0(r'_{ij}), \quad (2)$$

where the dimensionless length is defined as $r'_{ij} = r_{ij}/\lambda$. Further on, we will omit the primes and use the dimensionless form of the potential (2). The interaction force is then given by

$$\mathbf{F}_{ij} = -\nabla V_{ij} = (a * K_1(b * r_{ij}) - K_1(r_{ij}))\hat{\mathbf{r}}_{ij}, \quad (3)$$

where K_1 is a first order Bessel function, $\hat{\mathbf{r}}_{ij} = (\mathbf{r}_i - \mathbf{r}_j)/r_{ij}$, a and b are two positive coefficients.

The interaction potential Eq. (2) is generic: by choosing suitable parameters, it can be used as a model of non-monotonic interactions in different systems, for example, the well-known inter-atomic (molecule) Lennard Jones (LJ) potential: $\mu_{LJ}(r) = \mu_0[(r/\sigma)^{-12} - (r/\sigma)^{-6}]$. In Fig. 1(a), we compare the LJ potential for a particle of diameter $\sigma = 2.762\lambda$ and the energy unit $\mu_0 = 0.1V_0$ with the model potential given by Eq. (2) with the parameters: $a = 1.045 \times 10^7$, $b = 5.896$. The corresponding interaction forces are presented in Fig. 1(b). The comparison shows that the potentials and the corresponding forces (i.e., for the model potential (1) and the LJ potential) fairly agree with each other. On the other hand, one can easily see that the interaction potential Eq. (1) is a generalized form of the inter-vortex interaction in type-II superconductor which, as shown by Kramer²⁶, can be presented in the form: $V(r) = d_1(\kappa)K_0(r/\lambda) - d_2(\kappa)K_0(r/\xi)$.

The first term of Eq. (3) is repulsive while the second term describes an attractive interaction force. Indeed,

for $r \rightarrow \infty$, $K_1(x) \rightarrow \sqrt{\pi/(2x)}e^{-x}$. The interaction force (3) has a repulsive (attractive) tail when $b < 1$ ($b > 1$), while for $r \rightarrow 0$, $K_1(x) \rightarrow 1/x$ and thus $\mathbf{F}_{ij} \rightarrow (a/b - 1)/r$. Therefore, for short range the interaction force (3) is repulsive (attractive) when $a > b$ ($a < b$), and we only consider the case $a > b$ since an attractive interaction for short distances would result in a collapse of our system of point particles. When $a > b$ and $b < 1$, the interaction is always repulsive, and particles form a Wigner crystal structure. The most interesting case is realized when $a > b$ and $b > 1$, and the interaction has a repulsive core and attractive tail. In this case, there exists a critical distance r_c , where the inter-particle interaction energy (1) reaches a minimum (and the interaction force (3) changes sign). By setting the force equal to zero, the coefficient a is given by

$$a = \frac{K_1(r_c)}{K_1(b * r_c)}. \quad (4)$$

The pattern formation is determined by the coefficients b , r_c , and the particle density n .

We study pattern formation in a system of interacting particles using Langevin equations. The dynamics of a single particle i obeys the following overdamped equation of motion:

$$\eta \mathbf{v}_i = \mathbf{F}_i = \sum_{j \neq i} \mathbf{F}_{ij} + \mathbf{F}_i^T. \quad (5)$$

Here, η is the viscosity, which is set to unity. \mathbf{F}_{ij} is the interparticle interaction force defined by Eq. (3) and \mathbf{F}_i^T is the stochastic thermal force.

The thermal stochastic term \mathbf{F}_i^T in Eq. (5) obeys the following conditions:

$$\langle F_i^T(t) \rangle = 0 \quad (6)$$

and

$$\langle F_i^T(t) F_i^T(t') \rangle = 2\eta k_B T \delta_{ij} \delta(t - t'). \quad (7)$$

We consider a two-dimensional (2D) square simulation region $L_x \times L_y$ in the xy -plane and apply periodic boundary conditions in the x and y directions. For the interaction force given by Eq. (3), which exponentially decays for large distances, we use a cut-off for $r > 8$. The length of the square cell $L_x = L_y = L$ has been varied from 60 to 180 to examine the finite-size effects, and we set $L = 120$ to optimize the calculation speed without influencing the results. To obtain stable particle patterns, we performed simulated annealing simulations (SAS) of interacting particles. For this purpose, particles were initially randomly distributed inside the simulation region at some suitable non-zero temperature (depending on the inter-particle interaction). Then temperature was gradually reduced to zero, and the simulation was continued until a stable state was reached.

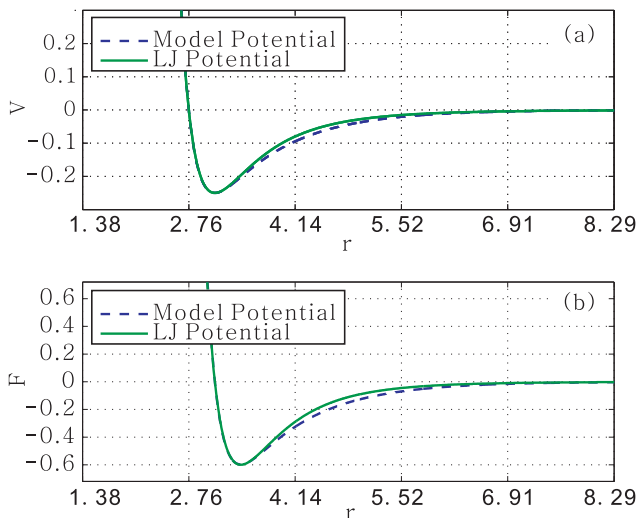


FIG. 1. (Color online) The LJ potential and the model potential given by Eq. (1) with the following parameters: $a = 1.045 \times 10^7$, $b = 5.896$, $\sigma = 2.762\lambda$, and $\mu_0 = 0.1V_0$ (a). The corresponding interaction forces (b).

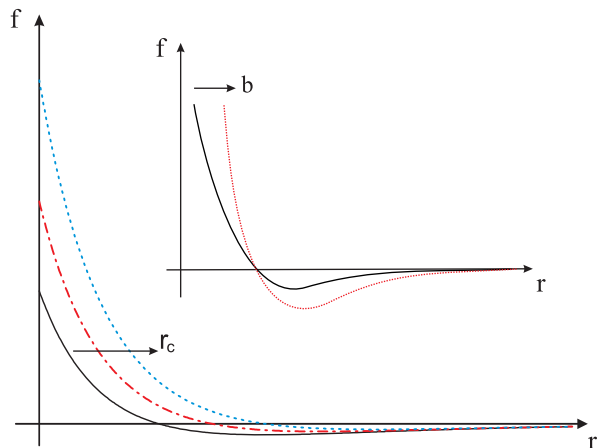


FIG. 2. (Color online) The profile of the inter-particle interaction force versus the distance. The main panel and the inset panel show the change in the force profile due to an increase of r_c and b , respectively.

III. PATTERNS AND PHASES

In this section we will study pattern formation and identify different phases depending on parameters of the interaction r_c , b and the particle density n . In Fig. 2, we illustrate the change of the interaction force profile due to the increase of r_c and b . On the one hand, the interaction force is very sensitive to r_c , since its increase directly leads to the increase of the repulsive part in Eq. (3) (see the main panel of Fig. 2). On the other hand, increase of b

leads to the increase of both the repulsive and attractive parts (see the inset of Fig. 2). However, the repulsive interaction increases much faster for $r < r_c$ than the attractive interaction for $r > r_c$.

Thus, with increasing b it becomes hard to reduce the inter-particle distance below r_c . In other words, the increase of b results in hardening of the core in the interaction force (3), i.e., the interaction changes continuously from a “soft-core” to a “hard-core” interaction.

A. Soft-core interaction

To analyze the soft-core regime, we set the coefficient $b = 1.1$. We define the critical density as $n_c = 8r_c^{-2}/\sqrt{3}$ which is the density of an ideal (hexagonal) Wigner crystal with the lattice constant $a = r_c$. The density is defined as $n = N/S$, where $S = 120 \times 120$ is the area of the simulation region and N is the number of particles (further on, when analyzing different patterns, we will refer to either the number of particles N in the simulation cell or to the density which is $n = N/14400$). For the case of $n < n_c$, which is considered here, the Wigner crystal is not stable due to the attractive interaction. In Fig. 3, we show patterns formed by $N = 1500$ particles when r_c increases from 1.9 (a) to 2.9 (f). Note that the condition $n < n_c$ is always fulfilled for all the values of r_c in this range. We found that for $r_c < 2.1$ particles form clusters similar to the formation of the “clump” phase found in Ref.^{16–18} (see Figs. 3(a) and (b)). The main difference to the patterns found in Ref.^{16–18} is that the relatively softer core in our case is compressed due to the attractive interaction, and the clusters acquire a circular shape. In addition, the interaction between the clusters (decaying exponentially for long distances) becomes negligible for inter-cluster distance of the order of few to several r_0 . Therefore, the clusters can be considered as non-interacting for low densities (although still they do not approach each other), contrary to the situation of Ref.^{16–18} when a super-lattice is formed due to the long-range cluster-cluster repulsion. When r_c increases, the clusters expand. In particular, for $r_c > 2.1$, the clusters start to elongate which is an indication of the instability with respect to the transition to the stripe phase. For $2.1 < r_c < 2.3$, a mixed state with both stripes and clusters is observed (see Fig. 3(c)). Further increase of r_c gradually destroys the cluster phase and leads to the formation of the labyrinth phase (see Figs. 3(d) to (f)).

In order to investigate the influence of the density, we gradually increase the number of particles from 1500 to 10500 in our simulation cell. First, in Fig. 4, we present patterns formed by $N = 5500$ particles for varying r_c . Note that $n > n_c$ for $N = 5500$. As compared to the lower density case shown in Fig. 3, in the cluster phase, the additional particles lead to the expansion of the clusters (see Figs. 4(a) and (b)). A mixture of clusters and stripes are formed when the additional particles form bridges connecting the clusters (see Fig. 4(c)) which will

be discussed in detail below. For the labyrinth phase (shown in Figs. 3(d) to (f) for $N = 1500$), the additional particles fill the empty regions (voids), resulting in the formation of the triangular lattice with varying local density (Fig. 4(d)) and, finally, a regular triangular lattice (see Figs. 4(e) and (f)). Note that the lattice with varying local density (Fig. 4(d)) is not stable in systems with pure repulsive interaction such as vortices in type-II superconductors.

We analyzed in detail the intermediate regime (i.e., corresponding to the transition from clusters to stripes, see Fig. 3(c)) where $r_c \approx 2.3$. The patterns for varying density are shown in Fig. 5. Fig. 5(a) displays a configuration at low density with $N = 1500$ when many individual clusters are formed. When increasing the density (see Fig. 5(b)), the clusters connect with each other and form a stripe phase. A further increase of the number of particles (Fig. 5(c)) results in the formation of a mixed phase of interconnected stripes with voids. A very interesting and counter-intuitive evolution is observed when the number of particles increases from $N = 5500$ to $N = 6500$ (see Fig. 5(d)): in contrast to the gradual transition from a void-rich configuration to a lattice-rich configuration when N changes from $N = 3500$ (b) to $N = 5500$ (c), in case of $N = 6500$ we observe a “reentrant” behavior, i.e., the void-rich phase starts to recover which is compensated by an increase of the local density in the stripes. However, further increasing density results in the expansion of the stripes to the empty regions which is accompanied by a decrease of the local density in the stripes, as shown in Fig. 5(e). The distribution of particles becomes more uniform, with only few small voids. Finally, for $N = 9500$ (Fig. 5(f)), we obtain a deformed triangular lattice characterized by a varying local density with only one small void.

Our calculations show that the obtained phases are very sensitive to variations in r_c . Thus, if r_c slightly decreases (e.g., $r_c = 2.25$), the number of clusters greatly increases as compared to the case $r_c = 2.3$, for the same density of particles. For $r_c = 2.25$, we also observe the transition from a void-rich configuration to a lattice-rich configuration. However, since the decrease of r_c increases the attractive component of the inter-particle interaction this occurs at much higher density. For even smaller values of r_c , i.e., $r_c < 2.1$, we do not observe the lattice phase, even for extremely large number of particles (up to $N = 20000$).

B. Phase Diagram

Based on the above analysis of the patterns and phases, we constructed a phase diagram in the plane of r_c and the number density n (see Fig. 6). For extremely low density ($n < 0.03$), particles form small clusters which are well separated, and the patterns are rather insensitive to variations of r_c . However, phases become richer when density n increases (i.e., $n > 0.1$). Low values of

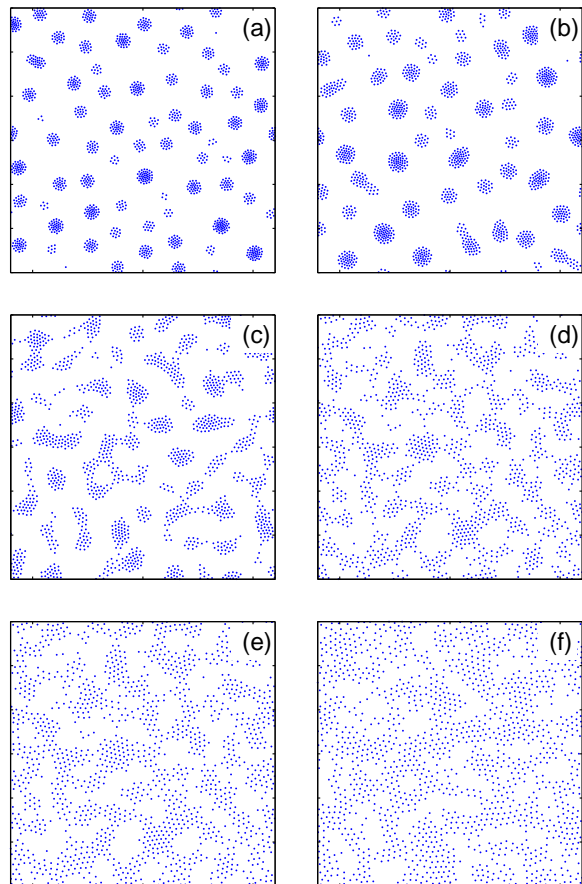


FIG. 3. (Color online) Different patterns for $N = 1500$ particles in a unit cell $L \times L$ with $L = 120$ for varying r_c : $r_c = 1.9$ (a), 2.1 (b), 2.3 (c), 2.5 (d), 2.7 (e), 2.9 (f).

r_c (i.e., $r_c < 2.1$) still favor cluster formation for a broad range of densities although the clusters become denser for large n . With increasing r_c , clusters become unstable with respect to the formation of “bridges” between separate clusters which is a precursor of the formation of stripes. Stripes are formed in a rather narrow range of r_c when $r_c > 2.1$ (see Fig. 6). The stripe phase is represented by two sub-phases, I and II, i.e., void-rich phase (see Fig. 6(i)) and void-poor (lattice-rich) phase (Fig. 6(j)). For larger r_c and $n < n_c$, particles form labyrinth structures. However, when increasing the density, additional particles fill the empty regions and finally they form a deformed triangular lattice with varying density. Depending on r_c and $n < n_c$ deformed lattice is characterized by a varying local density or by the appearance of voids. Correspondingly, we distinguish two regions (1 and 2 in Fig. 6). Note that in the vicinity of the phase boundaries patterns are always mixtures of the two phases (e.g., clusters and stripes) except the phase transition from the stripe phase to the deformed triangular lattice. Near this phase boundary, particles either form stripes with high local density or deformed triangular lattices with lower local density. The probability of

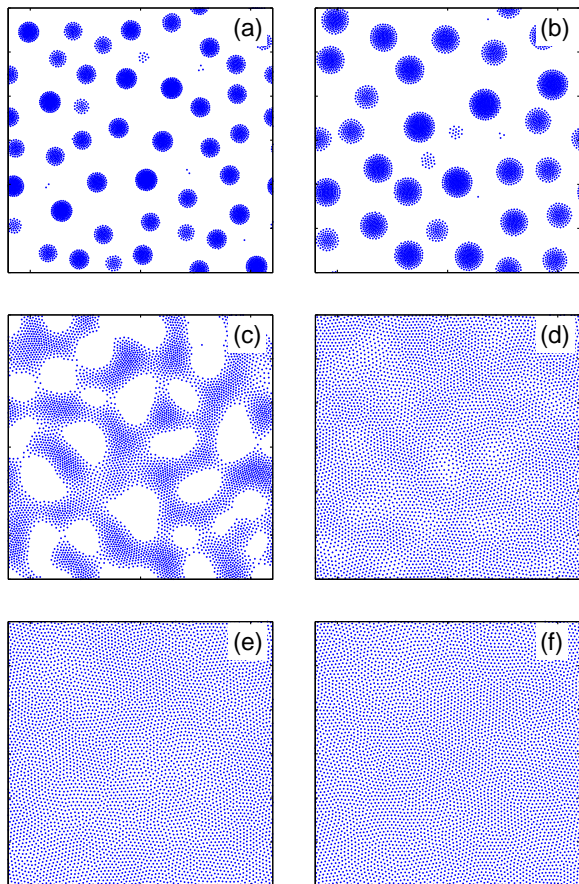


FIG. 4. (Color online) Patterns for $N = 5500$ particles in a unit cell $L \times L$ with $L = 120$ for varying r_c : $r_c = 1.9$ (a), 2.1 (b), 2.3 (c), 2.5 (d), 2.7 (e), 2.9 (f).

finding the lattice configuration greatly increases when r_c or n increases. Finally, for very large density, when the average interparticle distance becomes larger than r_c the repulsive interaction prevails resulting in the formation of an almost perfect triangular lattice.

The phases presented in Fig. 6 are found in many real systems. For example, the cluster phase is found in such systems as colloids^{10,12,19,20} and neutron stars². The obtained stripe patterns are very similar to those in Langmuir monolayers⁸.

Several of the calculated phases were found in superconductors, e.g., the stripe phase in the mixed state of type-I superconductors, clusters of Meissner phase or vortex clusters in the intermediate state in low- κ type-II superconductors^{27,28}, the labyrinth phase (i.e., vortex lattice with voids) or vortex clusters in type-1.5 superconductors²⁹. In spite of the variety of the physical systems and length scales ranging from nano- and micro-objects to cosmic objects, the common feature of all these systems is a competing attractive-repulsive interparticle interaction which allows analyzing them within the same approach.

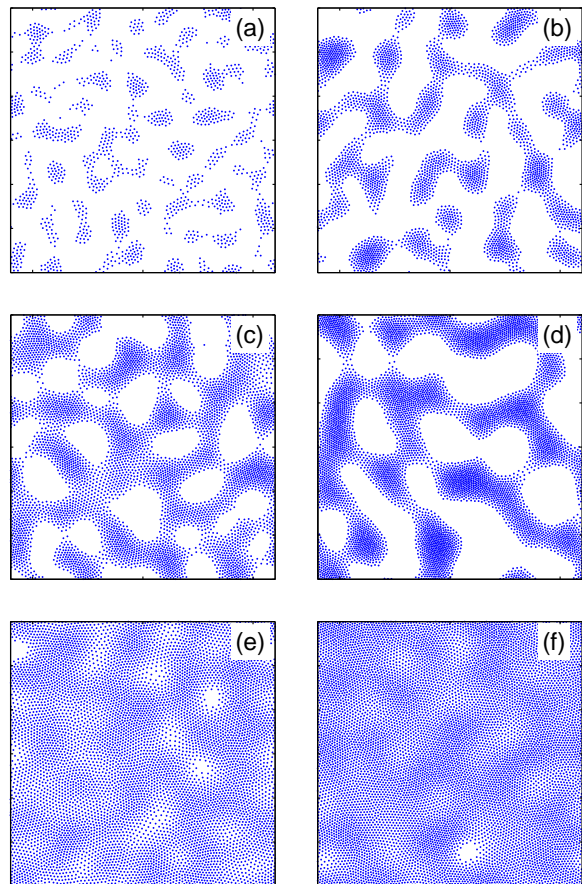


FIG. 5. (Color online) Patterns for $r_c = 2.3$ and varying number of particles N (in the computational unit cell $L \times L$ with $L = 120$): $N = 1500$ (a), 3500 (b), 5500 (c), 6500 (d), 7500 (e), 9500 (f).

C. Hard-core interaction

Let us now analyze the influence of coefficient b on the pattern formation. As mentioned above (see Fig. 2), an increase in b changes the potential from a soft-core to a hard-core. Hardening the repulsive core in the interaction potential generally leads to a decreasing compressibility of the inner parts of the patterns where particles are closely packed. Correspondingly, the patterns change as compared to the soft-core regime.

As shown in Fig. 7, for $b = 4$ and low density ($N = 1500$), all the patterns are clusters of different shape. Thus for $r_c = 1.15$ and $r_c = 1.3$, the clusters are of circular shape similar to those found in the soft-core regime although for $r_c = 1.3$ some clusters composed of a small number of particles have polygon shapes. With increasing r_c , polygon shaped clusters become more favorable, which allows us to identify them as short stripes. For even larger r_c , the clusters become much larger. They represent separate islands of triangular lattices.

For higher density ($N = 6500$), the variety of phases is much richer. Although for $r_c = 1.15$ circular-shape

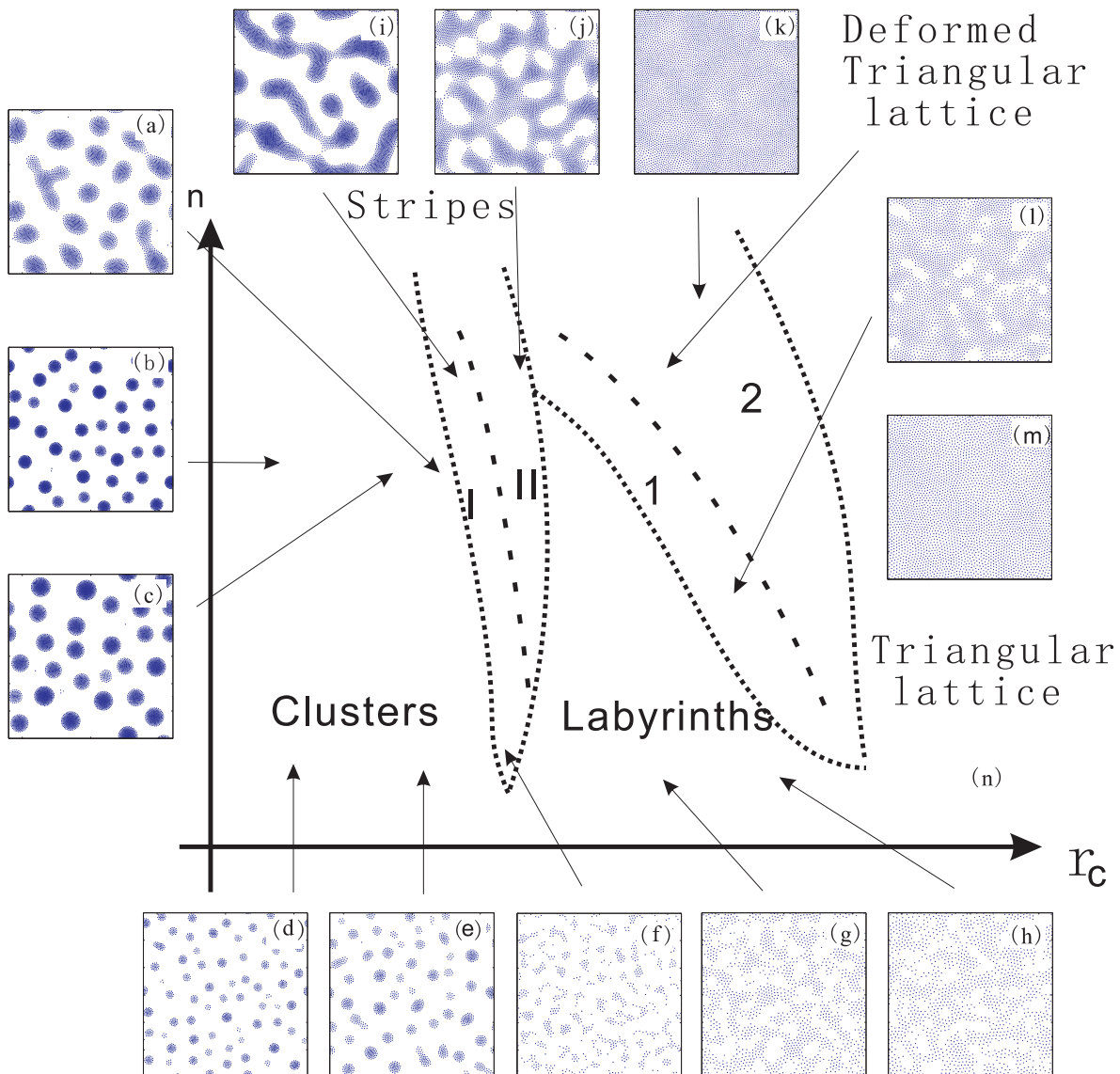


FIG. 6. (Color online) The phase diagram in the plane “critical radius r_c – density n ” (n) and representative patterns (a to m) for the different phases. For extremely low density ($n < 0.03$), particles form small well separated clusters. For $r_c < 2.1$, particles form clusters. For larger r_c , the size of the clusters increases (see the change from (d) to (e) and (b) to (c)). The increase of the density results in increasing the size of the clusters (see the change from (d) to (b) and (e) to (c)). Further increase of r_c leads to elongation of the clusters and the formation of “bridges” between them (a). Thus, the configurations change gradually from the cluster phase to the stripe phase (i). When r_c or n become even larger, stripes interconnect and form patterns with voids (j). Thus the stripe phase is divided into two sub-phases, I and II. When r_c become even larger, labyrinth-like configurations are formed for $n < n_c$ (see (g) and (f)). With further increase of r_c or n , deformed triangular lattice with (k) or without voids (l) are formed. The deformation of a triangular lattice is reduced for even larger values of r_c and n (m).

clusters are still observed (see Fig. 8(a)), which grow in size for $r_c = 1.3$ and slightly deviate in shape from circular (Fig. 8(b)), for larger $r_c = 1.45$ deviations of the cluster shape from circular become more pronounced (see Fig. 8(c)). With further increasing r_c , i.e., $r_c = 1.6$, stripes are formed (see Fig. 8(d)) followed by lattices with voids for $r_c = 1.75$ and $r_c = 1.9$. In the hard core regime, deformations of lattices occur via the appearance of voids instead of varying local density (in the soft-core regime).

IV. ANALYSIS OF THE PATTERNS

A. Radial Distribution Function

Although different patterns and phases studied above are qualitatively well distinguished, it is highly desirable to build a set of solid criteria which would allow us to identify them in a quantitative manner. For this purpose,

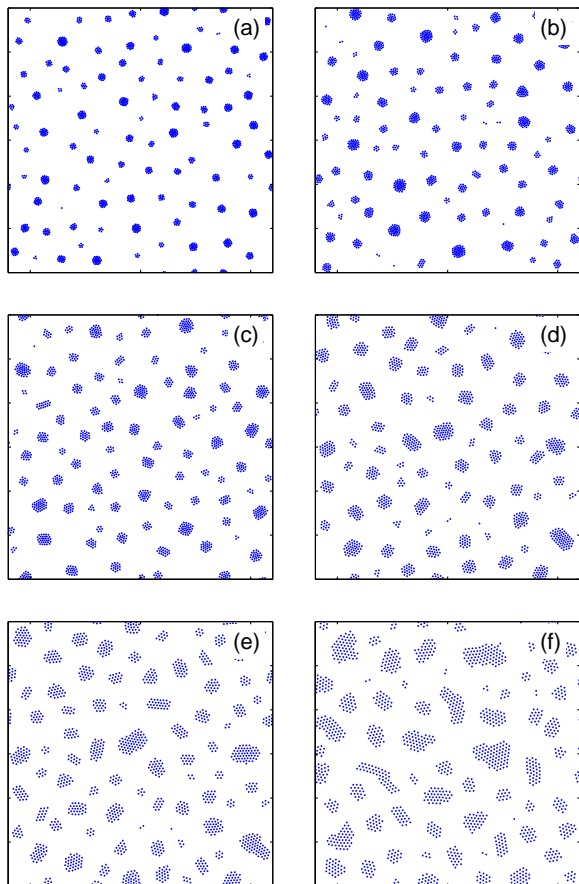


FIG. 7. (Color online) Patterns for $N = 1500$ particles in a unit cell $L \times L$ with $L = 120$, $b = 4$ and for varying r_c : $r_c = 1.15$ (a), 1.3 (b), 1.45 (c), 1.6 (d), 1.75 (e), 1.9 (f).

we analyze here different phases by means of the Radial Distribution Function (RDF). The RDF, $g(r)$, describes the variation of the atomic (particle) density as a function of the distance from one particular atom (particle). If we define an average density as $n = N/V$ (where V is the volume or surface area in the 2D case), then the local density at distance r is $ng(r)$. The knowledge of RDF is important since one can measure $g(r)$ experimentally using neutron scattering or x-ray diffraction scattering³⁴. Moreover, macroscopic thermodynamic quantities can be calculated using $g(r)$ in thermodynamics³⁵.

In our calculations, we define the RDF $g_i(r)$ as follows:

$$g_i(r) = \frac{\Delta N / \Delta r}{2\pi r}. \quad (8)$$

Here, the lower index indicates that the RDF centers at the position of the i th particle; ΔN is the number of particles whose distance to the i th particles is between r and $r + \Delta r$. The average $g(r)$ is given by

$$g(r) = \frac{1}{N} \sum_{i=1}^N g_i(r). \quad (9)$$

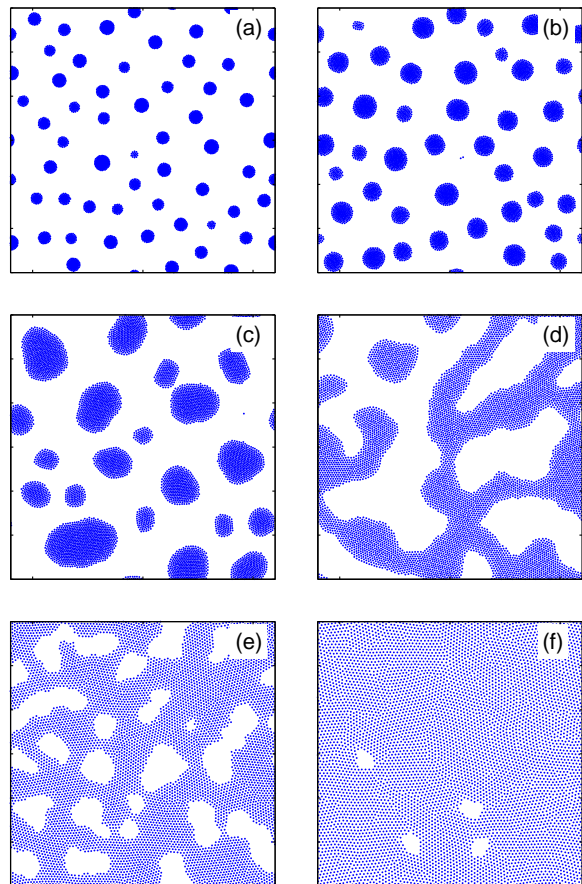


FIG. 8. (Color online) Patterns for $N = 6500$ particles in a unit cell $L \times L$ with $L = 120$, $b = 4$ and for varying r_c : $r_c = 1.15$ (a), 1.3 (b), 1.45 (c), 1.6 (d), 1.75 (e), 1.9 (f).

In Fig. 9(a), we plot the function $g(r)$ calculated for the low-density cluster configuration shown in Fig. 3(b). The function $g(r)$ has two well-pronounced peaks. The first peak corresponds to the average distance to the first coordination sphere (nearest neighbors) while the second one is located at the distance approximately twice the distance to the first peak, which shows short-range periodicity. For r larger than the size of the cluster, and smaller than the inter-cluster distance, $g(r) < 1$, since only few particles are located inside this range. As well as for the RDF obtained for the pasta phase in neutron stars², the decreasing tail in our case also shows a strong aggregation of the particles in the cluster phases. The minimum of $g(r)$ is very close to zero since most of the clusters have circular symmetry and they are well separated. The position of the minimum of $g(r)$ (marked by the gray arrow in Fig. 9(a)) gives an estimate of the average diameter of the clusters.

For the stripe phase (see Fig. 9(b) for the pattern shown in Fig. 3(d)), there are also two peaks indicating the short-range periodicity, similar to the cluster phase. However, unlike in the case of clusters the minimum of $g(r)$ is non-zero since the stripes are generally not sep-

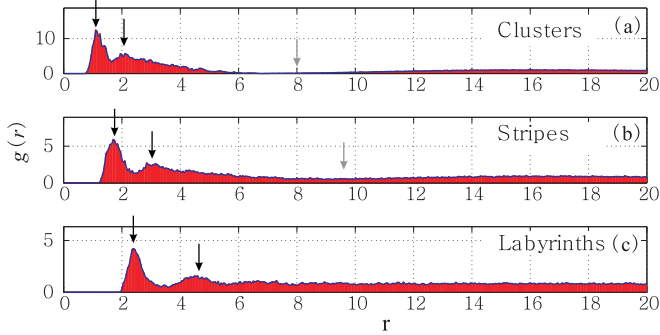


FIG. 9. (Color online) The average RDF of the patterns formed at low density ($N = 1500$). (a), (b), and (c) correspond to the patterns shown in Figs. 3(b), (d), and (f), respectively. The peaks marked by dark arrows show the short-range periodicity. The gray arrow shows the minimum of the RDF.

arated. For the labyrinth phase (see Fig. 9(c) for the pattern shown in Fig. 3(f)), only short-range periodic ordering exists, and $g(r)$ becomes uniform for larger r .

In Fig. 10, we plot $g(r)$ for the patterns formed at high density ($N=5500$). For clusters, the increase in the density leads to an increasing variation of the cluster size. Note, however, that the sizes of individual clusters are rather insensitive to moderate variations of the number of particles in the clusters, due to the strong compressibility of the core. As a result, the function $g(r)$ for the high density clusters misses the short-range periodicity and the second peak disappears (see Fig. 10(a)). Strikingly, this peak still exist for the void-rich phase (see Fig. 10(b)). The decrease of the tail of $g(r)$ becomes very slow, which shows a minor aggregation of the particles.

For the lattice phase (see Fig. 10(b)), the position of the first peak is $r_1 \approx a = \sqrt{2}/(\sqrt{3}n)$, where a is the distance between two neighboring particles in the ideal triangular lattice with the density n . The positions of the second and third peaks are at $r_2 \approx \sqrt{3}a$ and at $r_2 \approx 2a$, respectively, corresponding to those in a triangular lattice. A fourth, fifth and even sixth peaks appear, which shows that this phase is much more ordered. However, due to the variation of the local density, these peaks are strongly broadened, and they are actually a combination of many neighboring peaks. These peaks become clearer for larger r_c or n , which implies that the lattices become more regular.

It is interesting to compare the results of the function $g(r)$ for hard-core interaction with those for soft-core interaction. Although the clusters shown in Figs. 8(a) and (b) have shapes very similar to those of the clusters shown in Figs. 4(a) and (b), the analysis using the RDF shows that most of the clusters shown in Fig. 8(b) have hexagonal ordered cores. The peaks in $g(r)$ appear to be much better separated than for, e.g., the deformed triangular

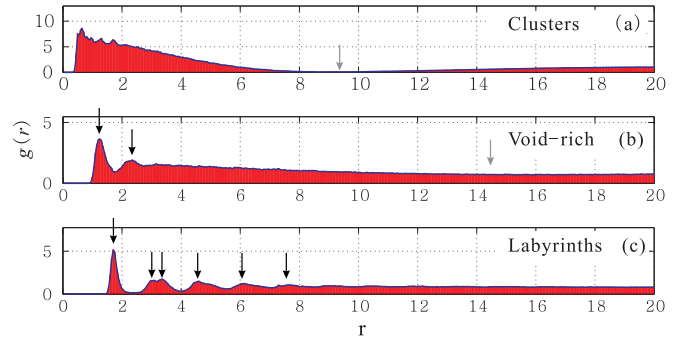


FIG. 10. (Color online) The average RDF of the patterns formed at high density ($N=5500$). (a), (b), and (c) correspond to the patterns shown in Figs. 4(b), (d), and (f), respectively. The arrows have the same meaning as in Fig. 9.

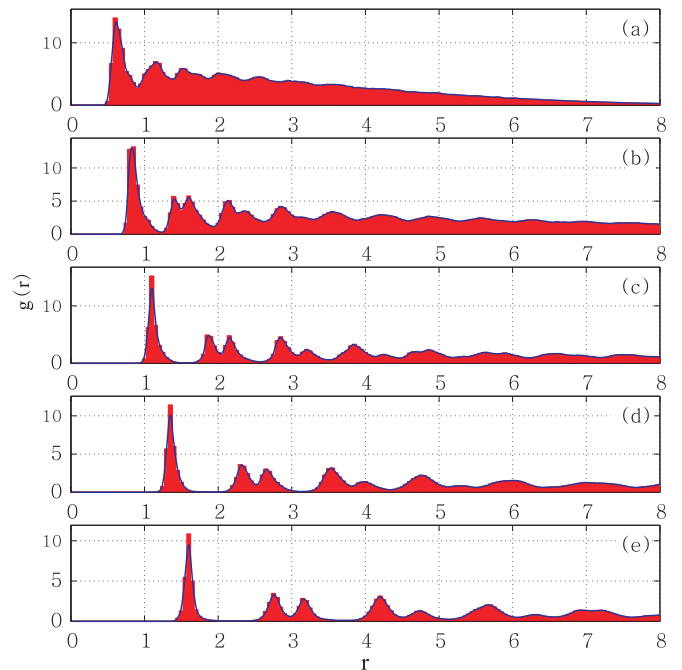


FIG. 11. (Color online) The average RDF of the patterns formed in the hard-core case. (a), (b), (c), (d), and (e) correspond to the patterns (a), (b), (c), (d), and (e) in Fig. 8, respectively.

lattice formed in the soft-core case (see Fig. 10(c)). For the stripe and void-rich phases, the RDF shows much clearer triangular lattice ordering.

Therefore, the analysis using the RDF allowed us to establish quantitative criteria for the different phases and reveal the differences in the structure of the patterns (which look similar, e.g., clusters) in case of soft- and hard-core interparticle interaction.

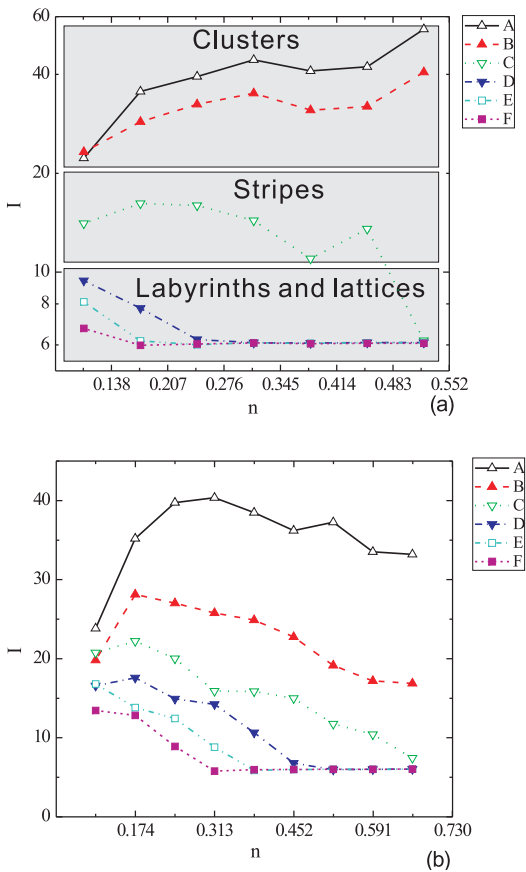


FIG. 12. (Color online) The average local density I versus the particle density n for $b = 1.1$ (a). Curves A, B, C, D, E, and F correspond to $r_c = 1.9, 2.1, 2.3, 2.5, 2.7,$ and 2.9 , respectively. For the cluster phase, $I > 20$, for the stripe phase, $10 < I < 20$, for the labyrinth phase, $6 < I < 10$. $I = 6$ for lattice and deformed lattice configurations. The local density I versus the number of particles N for $b = 4$ (b). Curves A, B, C, D, E, and F correspond to $r_c = 1.15, 1.3, 1.45, 1.6, 1.75,$ and 1.9 , respectively.

B. Local density

Let us define, using the RDF, an “order parameter” to characterize the different phases. By definition, the local density is:

$$I_i = \int_0^\xi 2\pi r n g_i(r) dr = N_\xi - 1. \quad (10)$$

Here, $N_\xi \approx \pi \xi^2 n$ is the average number of particles within the circle centered at the i th particle with radius $R = \xi$. Since in an ideal triangular lattice one particle has six nearest neighbors, we take $N_\xi = 7$, then $\xi = \sqrt{N_\xi/\pi n} = \sqrt{7/\pi n}$. Thus, for any configuration characterized by a small local density fluctuation, the average local density $I = \langle I_i \rangle = 6$. From the definition given by Eq. (10), we can see that the presence of a large fraction of empty regions can considerably increase

I since only the “shell” of those regions of thickness ξ is considered. In Fig. 12(a), we plot the function I for different r_c and N for the soft-core interaction with $b = 1.1$. We see that the function I can be used to characterize the different phases. Thus we found that, for clusters, I is always large ($I > 20$) since aggregation is strong. For stripes, aggregation is smaller, and thus I is smaller ($10 < I < 17$). For labyrinths, the regions free of particles are relatively small. Therefore, I ranges between 6 and 9. Finally, for the lattice phase, I is always 6. Therefore, the function I serves as a measure of the aggregation of particles and allows us to effectively distinguish the different phases.

The function I also provides a tool to analyze the stability of patterns with increasing density. This is demonstrated in Fig. 12(b), where we plot I for the hard-core case when $b = 4$. For $r_c = 1.15$, $I > 20$ for all the values of the density, and thus the clusters are stable. However, the situation changes for $r_c = 1.3$: while clusters are formed for low densities up to $N \approx 7500$, for larger density I decreases below the value $I = 20$ which means that clusters elongate and interconnect giving rise to the onset of the stripe phase. For $r_c = 1.45$, the particles start to form stripes at even lower density ($N=3500$). For higher density, the additional particles fill in the empty regions and finally they form the lattice phase. For $r_c > 1.6$, the island-like clusters formed at low densities are very unstable with respect to an increase in density. The additional particles rapidly occupy the empty regions, and the patterns change from clusters to stripes and from stripes to lattice with increasing density.

Therefore, the phenomenological description of pattern evolution with increasing density we revealed above in Sec. III.A has been verified in a quantitative manner using the rigid basis of the local density function approach.

C. Occupation factor

We demonstrated that the (average) RDF $g(r)$ (Eq. (9)) and the local density function I (Eq. (10)) allowed us to unambiguously characterize the different patterns and phases. At the same time, it is still hard to distinguish, using the above tools, between the labyrinth phase (or a lattice with voids) and the lattice phase (especially in the soft-core regime when the corresponding RDF does not differ much from each other, and both phases are characterised by small values of I). However, these phases can be easily distinguished by employing another simple criterion, namely, the occupation factor which characterizes the fraction of the space occupied by particles to the total space.

Let us assume that all the patterns are formed by islands of triangular lattice with the average distance between two nearest neighbor particles $r = r_1$, where r_1 is the position of the first peak of the RDF. Then the ratio of the area occupied by the particles and the whole simulation area is $A = (r_1/a)^2$. As shown in Fig. 13(a), this

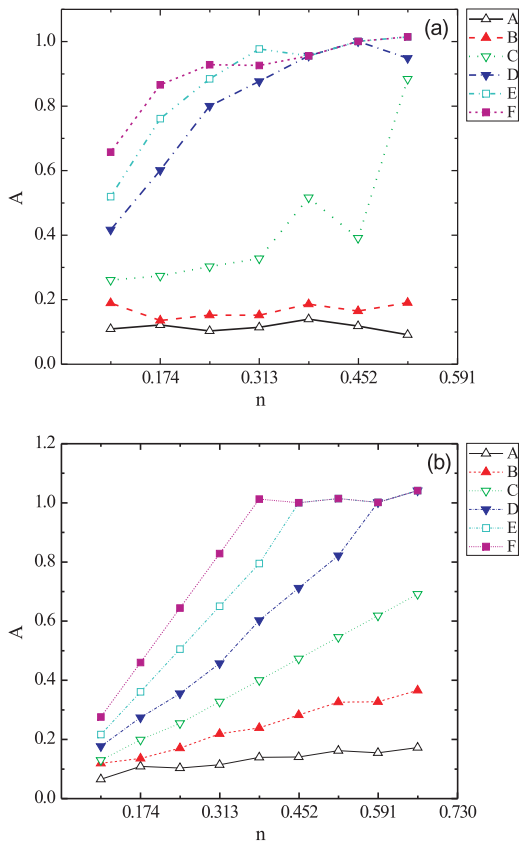


FIG. 13. (Color online) The occupation factor $A = (r_1/a)^2$ for $b = 1.1$ (a). Curves A, B, C, D, E, and F correspond to $r_c = 1.9, 2.1, 2.3, 2.5, 2.7,$ and 2.9 , respectively. The occupation factor, A for $b = 4$ (b). Curves A, B, C, D, E, and F correspond to $r_c = 1.15, 1.3, 1.45, 1.6, 1.75,$ and 1.9 , respectively.

ratio can be used to distinguish the labyrinth phase and the lattice phase, since for the lattice phase $A \approx 1$.

We also found that circular clusters in the case of soft-core interaction are very stable with respect to an increase in the density. In this case, the additional particles cannot efficiently increase the occupation factor due to the increase in the local density of the core. However, for the stripe and labyrinth phases, the occupation factor A increases with the density (see Fig. 13(a)). These phases are not stable for high density. Thus the large jump in $A(N)$ at $N = 6500$ in curve C in Fig. 13(a) shows the phase transition from the stripe phase to the lattice phase.

As one can expect, in the case of hard-core interaction, the occupation factor increases nearly linearly versus the density (see Fig. 13(b)). Therefore, the polygon shape and island-like clusters are not stable: with increasing density they evolve to the lattice phase (the plateau in $A(N)$ in Fig. 13(b)).

In addition, let us introduce another useful quantity which characterizes the degree of “perfection” of a lattice.

Let us define the particles with the inter-particle distance shorter than ξ as neighboring particles. Then

$$\begin{aligned} \varepsilon &= \frac{1}{a} \sqrt{\frac{\int_0^\xi 2\pi r g(r) n (r-a)^2 dr}{\int_0^\xi 2\pi r g(r) n dr}} \\ &= \frac{1}{a} \sqrt{\frac{\int_0^\xi r g(r) (r-a)^2 dr}{\int_0^\xi r g(r) dr}}. \end{aligned} \quad (11)$$

is an average displacement of the inter-distance between two neighbor particles (measured in units of a), which is independent of the density. The function ε is non-zero for a deformed triangular lattice and 0 for the ideal triangular lattice. Thus, ε quantitatively measures the degree of perfection of a lattice. Note that ε is only used for lattices as an auxiliary tool to distinguish ordered lattices from less ordered ones (see Table I).

V. CONCLUSIONS

Using molecular-dynamics simulations, we analyzed the pattern formation and identified different phases in a system of particles interacting via a non-monotonic potential, with a repulsive short-range part and attractive long-range part. The form of the interacting potential is generic: it describes, depending on specific parameters, the interparticle interaction in a variety of physical systems ranging from, e.g., atoms and molecules (Lennard-Jones potential) to colloids and neutron stars. It can also be used as a model of inter-vortex interaction in low κ type-II superconductors and in recently discovered so-called “type-1.5” superconductors. The obtained different phases were summarized in a phase diagram in the plane “critical radius r_c – density n ” (r_c is the critical radius where the interaction force changes its sign). We also analyzed the influence of the hardness of the “core”, i.e., the strength of the repulsive core part of the interaction potential on the pattern formation.

We developed a set of criteria in order to unambiguously identify the obtained phases using the following approaches: (i) the Radial Distribution Function (RDF) $g(r)$, (ii) the local density function I , and (iii) the occupation factor A . In addition, we introduced a parameter which characterizes the degree of perfection of a lattice ε . Employing these approaches, we elaborated the criteria for the identification of the different phases which are summarized in Table I.

VI. ACKNOWLEDGMENTS

We acknowledge fruitful discussions with Ernst Helmut Brandt. This work was supported by the “Odysseus” Program of the Flemish Government and the Flemish Science Foundation (FWO-VI), the Interuniversity Attraction

Patterns	$g(r)$	I	A	ε
clusters	peak at $r_1(r_2)$, $g(r)_{min} = 0$	> 20		
stripes	peak at $r_1(r_2)$, $g(r)_{min} > 0$	$10 \sim 20$		
labyrinths	peak at $r_1(r_2)$, $g(r) \approx \text{const}, r > r_2$	$6 \sim 10$	< 1	
lattice	several peaks: $r_1, r_2 \dots$	≈ 6	≈ 1	0
deformed lattice	several peaks: $r_1, r_2 \dots$	≈ 6	≈ 1	> 0

TABLE I. The set of criteria used to quantitatively identify the different phases in terms of the RDF $g(r)$, the local density function I , the occupation factor A , and the parameter ε (for details, see the text).

tion Poles (IAP) Programme — Belgian State — Belgian Science Policy, and the FWO-VI.

- ¹ E. Y. Vedmedenko, *Competing interactions and patterns in nanoworld* (WILEY-VCH Verlag GmbH & Co. KGaA, 2007).
- ² C. J. Horowitz, M. A. Pérez-García, and J. Piekarewicz, Phys. Rev. C **69**, 045804 (2004).
- ³ M. F. Islam, K. H. Lin, D. Lacoste, T. C. Lubensky, and A. G. Yodh, Phys. Rev. E **67**, 021402 (2003).
- ⁴ D. Lacoste and T. C. Lubensky, Phys. Rev. E **64**, 041506 (2001).
- ⁵ R. E. Rosensweig, M. Zahn, and R. Shumovich, J. Magn. Magn. Mater. **39**, 127 (1983).
- ⁶ A. Tsebers and M. Maiorov, Magnetohydrodynamics (New York) **16**, 21 (1980).
- ⁷ V. M. Kaganer, H. Möhwald, and P. Dutta, Rev. Mod. Phys. **71**, 779 (1999).
- ⁸ K. A. Suresh, J. Nittmann, and F. Rondelez, Europhys. Lett. **6**, 437 (1988).
- ⁹ G. R. Berdiyrov, A. D. Hernandez, and F. M. Peeters, Phys. Rev. Lett. **103**, 267002 (2009).
- ¹⁰ N. Hoffmann, F. Ebert, C. N. Likos, H. Löwen, and G. Maret, Phys. Rev. Lett. **97**, 078301 (2006).
- ¹¹ P. J. Lu, E. Zaccarelli, F. Ciulla, A. B. Schofield, F. Sciortino, and D. A. Weitz, Nature **453**, 499 (2008).
- ¹² A. I. Campbell, V. J. Anderson, J. S. van Duijneveldt, and P. Bartlett, Phys. Rev. Lett. **94**, 208301 (2005).
- ¹³ C. L. Klix, C. P. Royall, and H. Tanaka, Phys. Rev. Lett. **104**, 165702 (2010).
- ¹⁴ F. F. Munarin, K. Nelissen, W. P. Ferreira, G. A. Farias, and F. M. Peeters, Phys. Rev. E **77**, 031608 (2008).
- ¹⁵ M. Seul and D. Andelman, Science **267**, 476 (1995), <http://www.sciencemag.org/content/267/5197/476.full.pdf>.
- ¹⁶ C. Reichhardt, C. J. Olson, I. Martin, and A. R. Bishop, Europhys. Lett. **61**, 221 (2003).
- ¹⁷ C. Reichhardt, C. J. O. Reichhardt, I. Martin, and A. R. Bishop, Phys. Rev. Lett. **90**, 026401 (2003).
- ¹⁸ C. Reichhardt, C. J. O. Reichhardt, and A. R. Bishop, Europhys. Lett. **72**, 444 (2005).
- ¹⁹ F. Sciortino and P. Tartaglia, Adv. Phys. **54**, 471 (2005).
- ²⁰ F. Sciortino, S. Mossa, E. Zaccarelli, and P. Tartaglia, Phys. Rev. Lett. **93**, 055701 (2004).
- ²¹ X. B. Xu, H. Fangohr, S. Y. Ding, F. Zhou, X. N. Xu, Z. H. Wang, M. Gu, D. Q. Shi, and S. X. Dou, Phys. Rev. B **83**, 014501 (2011).
- ²² M. Tarzia and A. Coniglio, Phys. Rev. Lett. **96**, 075702 (2006).
- ²³ M. Tarzia and A. Coniglio, Phys. Rev. E **75**, 011410 (2007).
- ²⁴ S. Mossa, F. Sciortino, P. Tartaglia, and E. Zaccarelli, Langmuir **20**, 10756 (2004), <http://pubs.acs.org/doi/pdf/10.1021/la048554t>.
- ²⁵ A. de Candia, E. Del Gado, A. Fierro, N. Sator, M. Tarzia, and A. Coniglio, Phys. Rev. E **74**, 010403 (2006).
- ²⁶ L. Kramer, Phys. Rev. B **3**, 3821 (1971).
- ²⁷ E. H. Brandt and U. Essmann, phys. stat. sol. (b) **144**, 13 (1987).
- ²⁸ E. Brandt and M. Das, J. Supercond. Novel Magn. **24**, 57 (2011), [10.1007/s10948-010-1046-8](https://doi.org/10.1007/s10948-010-1046-8).
- ²⁹ V. Moshchalkov, M. Menghini, T. Nishio, Q. H. Chen, A. V. Silhanek, V. H. Dao, L. F. Chibotaru, N. D. Zhigadlo, and J. Karpinski, Phys. Rev. Lett. **102**, 117001 (2009).
- ³⁰ A. Chaves, L. Komendová, M. V. Milošević, J. S. Andrade, G. A. Farias, and F. M. Peeters, Phys. Rev. B **83**, 214523 (2011).
- ³¹ L. Komendová, M. V. Milošević, M. V. Shantenko, and F. M. Peeters, Phys. Rev. B (2011), [arXiv:1106.1080](https://arxiv.org/abs/1106.1080).
- ³² E. Babaev and M. Speight, Phys. Rev. B **72**, 180502 (2005).
- ³³ V. R. Misko, D. Bothner, M. Kemmler, R. Kleiner, D. Koelle, F. M. Peeters, and F. Nori, Phys. Rev. B **82**, 184512 (2010).
- ³⁴ F. Hajdu, S. Lengyel, and G. Pálinkás, J. Appl. Cryst. **9**, 134 (1976).
- ³⁵ D. Frenkel and B. Smit, *Understanding molecular simulation : from algorithms to applications*, 2nd ed. (Academic Press, 2002).